Time-dependent aspects of electron degradation. V. Ar-H_2 mixtures

Ken-ichi Kowari,* and Mitio Inokuti
Argonne National Laboratory, Argonne, Illinois 60439

Mineo Kimura
Argonne National Laboratory, Argonne, Illinois 60439
and Department of Physics, Rice University, Houston, Texas 77251
(Received 20 November 1989)

Time-dependent electron degradation spectra and yields of initial products are studied for the Ar-H_2 mixture by using the time-dependent Spencer-Fano (TDSF) theory. An integral form of the TDSF equation is derived and applied in numerical solutions. The present study shows, in the time-dependent context, that addition of a small amount of H_2 in Ar greatly enhances the yield of the triplet states of H_2 because of the presence of subexcitation electrons whose energies are below the electronic excitation threshold of Ar. The production of the triplet states is slow; it takes a period ten times longer than fast processes such as ion production. Secondary processes such as ion-molecule reactions following the electron degradation process are also discussed.

I. INTRODUCTION

It is known that the addition of a minute amount of any impurity to He gas remarkably increases the ionization yield due to ionizing radiation.[1-4] This spectacular increase, called the Jesse effect,[5] is partly due to the Penning ionization by which excited states of He ionize impurity atoms or molecules. Platzman[6] pointed out that also subexcitation electrons, whose energies are lower than the lowest electronic excitation energy of He, are capable of ionizing impurity atoms or molecules.

By contrast, the addition of a small amount of H_2 to Ar causes no spectacular increase of the ionization yield, as shown by experiment. A mixture of this type is called regular.[7-9] The lowest excited states of Ar are lower than the ionization energy of H_2, and therefore no Penning ionization occurs. No subexcitation electrons can ionize H_2 because of the similarity of ionization potentials of H_2 and Ar. However, some the the subexcitation electrons have enough energy to excite the lowest triplet excited state of H_2, and therefore we expect to see some effect of the subexcitation electrons on the yield of that state. Although the yields of ions[10,11] and of excited states[12] in the Ar-H_2 mixtures have been extensively studied, no particular attention has been paid to the role of the subexcitation electrons in previous studies.

The recent generalization of the Spencer-Fano theory to time-dependent cases[13-16] was stimulated by measurements related to temporal aspects of electron degradation phenomena using short-pulse radiolysis.[17-22] Time-dependent aspects of the degradation of subexcitation electrons have been studied[23-26] in N_2, CO_2, O_2, and H_2O. Time-dependent electron degradation spectra in high-energy regions have been studied[13,16] for pure Ar and pure H_2. The present study is a follow-up of those studies, now extended to the mixture of H_2 and Ar. Furthermore, we present a new element of theory, i.e., an integral equation for the time-dependent degradation spectrum, which is useful for numerical calculations.

II. THEORY

The Spencer-Fano theory including the recent extension to time-dependent cases was fully described earlier.[15] We give here a brief summary necessary for later discussion and also present an alternative form of the time-dependent Spencer-Fano equation.

A. Cross sections

For simplicity of discussion, let us first consider electron degradation in a pure gas, i.e., a gas consisting of a single species of molecules, having a single ionization energy I. We denote by $\sigma_s(T)$ the cross section for the excitation of the sth discrete state at excitation energy E_s by an electron of energy T. We denote by $\sigma_i(T)$ the ionization cross section, which is the integral of the differential ionization cross section $d\sigma_i(T,E)/dE$:

$$\sigma_i(T)=\int_I^{(T+I)/2} dE \frac{d\sigma_i(T,E)}{dE} , \tag{1}$$

where E represents the energy transfer. The total inelastic-collision cross section $\sigma_{\rm tot}(T)$ is given by

$$\sigma_{\rm tot}(T)=\sigma_i(T)+\sum_s \sigma_s(T) . \tag{2}$$

In numerical calculations we use the same cross-section data as in earlier studies.[10-12]

B. Time-independent Spencer-Fano equation

First, let us define the cross-section operator[15] K_T as

$$K_T y(T)=\sum_s \sigma_s(T+E_s)y(T+E_s) + \int_I^{\lambda} dE \frac{d\sigma_i(T+E,E)}{dE} y(T+E) + \int_{2T+I}^{T_0} dT' \frac{d\sigma_t(T',T+I)}{dE} y(T') - \sigma_{\text{tot}}(T)y(T) , \quad (3)$$

where λ represents the smaller of $T+I$ and T_0-T. For the treatment of atoms or molecules with several shells, (e.g., Ar), Eq. (3) must be generalized, as explicitly given in Eq. (5) of Kowari, Kimura, and Inokuti.[27]

The degradation spectrum $y(T)$ (total track length per unit range of energy T) obeys the Spencer-Fano equation

$$nK_T y(T)+u(T)=0 , \quad (4)$$

where $u(T)$ is the number of source electrons per unit range of energy T, and n is the number density of molecules in the medium. If the incident electron is monoenergic at energy T_0, we set $u(T)=\delta(T-T_0)$, write the corresponding solution $y(T_0,T)$, and call it the standard solution.

Once we obtain the degradation spectrum by solving Eq. (4), we can calculate the mean yield of the sth discrete state as

$$N_s(T_0)=n\int_{E_s}^{T_0} y(T_0,T)\sigma_s(T)dT . \quad (5)$$

The ionization yield $N_i(T_0)$ is similarly obtained as

$$N_i(T_0)=n\int_{I}^{T_0} y(T_0,T)\sigma_i(T)dT . \quad (6)$$

Let us introduce the time-independent Spencer-Fano equation for the mixture of A and B molecules. Let us denote the cross-section operator for A molecules as K_T^A and that for B molecules as K_T^B. The operator K_T^A is defined by Eq. (3), where all the cross sections refer to the A molecule. The operator K_T^B likewise refers to the B molecule. Then the time-independent Spencer-Fano equation for the mixture is

$$n_A K_T^A y(T)+n_B K_T^B y(T)+u(T)=0 , \quad (7)$$

where n_A is the number density of A molecules and n_B that of B molecules. For simplicity of later discussion, we may rewrite Eq. (7) in the same form as Eq. (4), with the redefinition of K_T by

$$nK_T=n_A K_T^A+n_B K_T^B , \quad (8)$$

where

$$n=n_A+n_B . \quad (9)$$

C. Time-dependent Spencer-Fano equation

The *incremental* degradation spectrum[15] $z(T;t)$ represents the rate of increase of the tracklength at energy T and at time t. It obeys the equation

$$v_T^{-1}\frac{\partial z(T;t)}{\partial t}=nK_T z(T;t)+u(T;t) , \quad (10)$$

where v_T is the speed of an electron with kinetic energy T, and $u(T;t)$ is the source strength per unit time at energy T and at time t.

If the source is monoenergetic at T_0 and is a sharp pulse at t_0, we set $u(T;t)=\delta(T-T_0)\delta(t-t_0)$. We call the solution of Eq. (10) with this $u(T,t)$ the standard solution and represent it as $z(T_0,T;t_0,t)$.

Let us consider the *cumulative* degradation spectrum,[15] defined as

$$Z(T;t)=\int_{-\infty}^{t} dt' z(T;t') . \quad (11)$$

Integrating Eq. (10) over t, we find that $Z(T;t)$ obeys the equation

$$v_T^{-1}\frac{\partial Z(T;t)}{\partial t}=nK_T Z(T;t)+U(T;t) , \quad (12)$$

where

$$U(T;t)=\int_{-\infty}^{t} dt' u(T;t') . \quad (13)$$

We express the standard solution as $Z(T_0,T;t_0,t)$. The cumulative yield for the standard solution is given as

$$N_s(T_0,T;t_0,t)=n\int_{E_s}^{T_0} Z(T_0,T;t_0,t)\sigma_s(T)dT . \quad (14)$$

D. Integral-equation form of the time-dependent Spencer-Fano equation

Let us recast Eq. (12). We multiply both sides of Eq. (12) by v_T and obtain

$$\frac{\partial Z(T;t)}{\partial t}=nv_T K_T Z(T;t)+v_T U(T;t) . \quad (15)$$

We add $AZ(T;t)$ to both sides of Eq. (15); here A is an arbitrary linear operator independent of t, but possibly dependent on T. Then we obtain

$$\frac{\partial Z(T;t)}{\partial t}+AZ(T;t)=X(T;t) , \quad (16)$$

where

$$X(T;t)\equiv(nv_T K_T+A)Z(T;t)+v_T U(T;t) . \quad (17)$$

In Eq. (16), e^{At} is an integrating factor. In other words, Eq. (16) is equivalent to

$$\frac{\partial}{\partial t}[e^{At}Z(T;t)]=e^{At}X(T;t) . \quad (18)$$

Treating temporarily $X(T;t)$ as known, we may formally solve this to obtain

$$Z(T;t)=e^{-At}\int_{-\infty}^{t} dt' e^{At'}X(T;t') . \quad (19)$$

Inserting here the definition of $X(T;t)$ of [Eq. (17)], we obtain

$$Z(T;t)=e^{-At}\int_{-\infty}^{t} dt' e^{At'}[(nv_T K_T+A)Z(T;t') + v_T U(T;t')] . \quad (20)$$

This is an integral equation for $Z(T;t)$; it may be viewed as an alternative form of the time-dependent Spencer-

Fano equation, Eq. (15).

A particular choice of A, viz.,

$$A = n v_T \sigma_{\text{tot}}(T) , \tag{21}$$

is useful for applications, where $\sigma_{\text{tot}}(T)$ is the cross section for inelastic scattering of an electron of energy T. To be more precise, we may define it by

$$\sigma_{\text{tot}}(T) = \int dT'' \sigma(T \to T'') , \tag{22}$$

where $\sigma(T \to T'')$ is the cross section for all processes by which an electron of energy T is lost and an electron of energy T'' is generated. Then $-AZ(T;t)$ represents the number of electron that have left from energy T by time t, and $(nv_T K_T + A)Z(T;t)$ the number of electrons that have arrived at energy T by time t.

E. Remarks on the integral equation

To see the meaning of the integral equation, let us consider a special case where $X(T;t)$ is set at

$$X(T_0;t) = \begin{cases} v_{T_0}\delta(T - T_0) & \text{for } t_0 < t \\ 0 & \text{for } t \le t_0 . \end{cases} \tag{23}$$

Then Eq. (19) leads to

$$\begin{aligned} Z(T_0, T; t_0, t) &= e^{-At} \int_{t_0}^{t} dt' e^{At'} v_{T_0} \delta(T - T_0) \\ &= A^{-1}(1 - e^{-A(t-t_0)}) v_{T_0} \delta(T - T_0) . \end{aligned} \tag{24}$$

This actually applies in the interval $T_0 - E_1 < T < T_0$, where E_1 is the lowest discrete excitation energy, and it provides a starting point for numerical calculations.

Next we perform a partial integration in Eq. (19) to obtain

$$\begin{aligned} &\int_{-\infty}^{t} dt' e^{At'} X(T;t') \\ &\quad = A^{-1} \left[e^{At} X(T;t) - \int_{-\infty}^{t} dt' e^{At'} x(T;t') \right] , \end{aligned} \tag{25}$$

where

$$\begin{aligned} x(T;t') &= \frac{\partial}{\partial t} X(T;t') \bigg|_{t=t'} \\ &= (nv_T K_T + A) z(T;t') + v_T u(T;t') . \end{aligned} \tag{26}$$

Thus we rewrite Eq. (19) as

$$Z(T;t) = A^{-1} \int_{-\infty}^{t} dt' [1 - e^{-A(t-t')}] x(T;t') . \tag{27}$$

It is instructive to compare this with Eq. (24). The quantity $x(T;t)$ represents the rate of production of all the electrons with energy T at time t. The kernel $A^{-1}\{[1 - \exp[-A(t-t')]\}$ with A given by Eq. (21) represents the probability that an electron produced at time t' suffers at least a collision by time t. Equation (27) may be viewed as a superposition of Eq. (24) with weight $x(T;t)$.

Finally, the incremental spectrum also satisfies Eq. (10), which is of the same form as Eq. (15). Thus the procedure of Sec. II D applies. Therefore the incremental spectrum satisfies the integral equation

$$\begin{aligned} z(T;t) = e^{-At} \int_{-\infty}^{t} dt' e^{At'} [&(nv_T K_T + A) z(T;t') \\ &+ v_T u(T;t')] . \end{aligned} \tag{28}$$

III. NUMERICAL PROCEDURES

Throughout the present work we treat gases at a total pressure of 1 atm and at a temperature of 0 °C. Results thereby obtained can be readily converted to other pressures and temperatures so long as they introduce no substantial change of physics apart from the number density of molecules n. The density n appears in the fundamental equation, Eq. (10), only as the coefficient of K_T. Therefore the product nt is the variable that governs the time dependence of the solution.

The energy mesh size used for solving Eq. (4), the time-independent Spencer-Fano equation, is 1 eV above 20 eV and 0.5 eV below 20 eV. We use Eq. (20), the integral equation of the time-dependent Spencer-Fano equation, for numerical calculations. The energy mesh size for Eq. (20) is the same as that for Eq. (4). The time-step size used for solving the time-dependent equation is 0.1 ns for H_2 and 0.05 ns for Ar. The time-step size for the mixture is 0.05 ns up to 16 ns. By 16 ns the cumulative degradation spectrum for the mixture reaches the stationary spectrum at electron energies above 16 eV. After 16 ns we calculate the cumulative degradation spectrum below energy of 16 eV only and use the time-step size of 0.5 ns.

IV. RESULTS AND DISCUSSION

A. Stationary case

We show the yields of products in Table I for H_2, in Table II for Ar, and in Table III for the Ar-H_2 mixture. To test the accuracy of the present calculations, we compare our results with those by Douthat.[28] Although the incident energy of an electron in our calculation is 2 keV and that in Douthat's is 10 keV,

$$W(T_0) = T_0 / N_i(T_0) \tag{29}$$

TABLE I. Yields of products of an electron at initial energy $T_0 = 2$ keV in H_2. The designation of the product species follows Douthat (Ref. 28).

Product species s	Threshold excitation energy E_s (eV)	Yield $N_s(T_0)$
Ions	16.1	58.5
Lyman	12.5	18.5
Werner	13.0	21.4
H($2\,^2P$)	14.9	1.10
Slow H($2\,^2S$)	15.3	5.78
Fast H($2\,^2S$)	32.9	1.01
$H(n=3)$	15.0	0.67
$H(n \ge 4)$	14.5	2.38
Triplets	8.8	21.7

TABLE II. Yields of products of an electron at initial energy $T_0=2$ keV in Ar. The designation of the six groups of excited states follows Eggarter (Ref. 29).

Product species s	Threshold Excitation Energy E_s (eV)	Yield $N_s(T_0)$
Ions		
M shell	15.76	73.4
L shell	250	0.573
Excited states		
I	11.79	13.8
II	14.25	4.95
III	14.97	2.75
IV	15.48	2.88
V	12.0	2.00
VI	12.8	8.71

and

$$G_s(T_0)=(100/T_0)N_s(T_0) \tag{30}$$

are virtually independent of T_0 in this high-energy region. The present W value for H_2 of 34.2 eV agrees with that of Douthat within 1%. The G value for the $b\,^3\Sigma_u^+$ excitation shows the largest discrepancy of 6%.

When a small amount of H_2 is added to Ar, the most remarkable result is seen in the yield 10.8 of $b\,^3\Sigma_u^+$, which is half the yield of the same species in pure H_2, as shown in Table III. It is usually expected that in the Ar(0.99)-H_2(0.01) mixture the yields of Ar products should be very close to those in pure Ar and that those of H_2 products should be very small. The threshold energy of $b\,^3\Sigma_u^+$, the lowest electronic excitation state of H_2, is 8.8 eV, and that of Ar is 11.8 eV. Therefore electrons in the energy range between 8.8 and 11.8 eV can lose their energies only through $b\,^3\Sigma_u^+$ excitation, apart from momentum transfer to Ar upon elastic scattering. This explains the remarkably large yield of $b\,^3\Sigma_u^+$ in the mixture.

TABLE III. Yields of products of an electron at initial energy $T_0=2$ keV in the mixture of Ar (0.99 in number fraction) and H_2 (0.01 in number fraction). The designation of the product species follows Douthat (Ref. 28) for H_2 and Eggarter (Ref. 29) for Ar.

Product species s	Threshold excitation energy E_s (eV)	Yield $N_s(T_0)$
Ar ions		
M shell	15.76	73.1
L shell	250	0.571
Ar excited states		
I	11.79	13.2
II	14.25	4.92
III	14.97	2.74
IV	15.48	2.87
V	12.0	1.88
VI	12.8	8.58
H_2 ions (H_2^+ and H^+)	16.1	0.196
Other products from H_2		
Lyman	12.5	0.0900
Werner	13.0	0.0930
$H(2\,^2P)$	14.9	0.003 87
Slow $H(2\,^2S)$	15.3	0.0224
Fast $H(2\,^2S)$	32.9	0.003 32
$H(n=3)$	15.0	0.002 40
$H(n=4)$	14.5	0.008 39
Triplets	8.8	10.8

B. Time-dependent case

1. *Cumulative spectra for pure H_2, pure Ar, and the Ar-H_2 mixture*

Figure 1 shows the cumulative spectrum for *pure* H_2 at different times. At 2 ns the cumulative spectrum shows a rapid decrease at energies immediately below the source energy. At earliest times, only the primary electron degrades and contributes to the spectrum between T_0 and $(T_0-I)/2$. The increase of the spectrum in the low-energy region is due to the contribution from secondary electrons. As time passes, more and more secondary electrons accumulate, and the cumulative degradation spectrum over the entire energy range approaches the stationary degradation spectrum.

The general trends of the cumulative degradation spectrum for pure Ar seen in Fig. 2 are similar to those for H_2; therefore we concentrate on points particular to Ar and on differences from H_2. As time passes, the cumulative spectrum for Ar approaches the stationary spectrum much faster than does that for H_2 because at the same number density the number of collisions for Ar is larger by two to three times than that for H_2 in the entire ener-

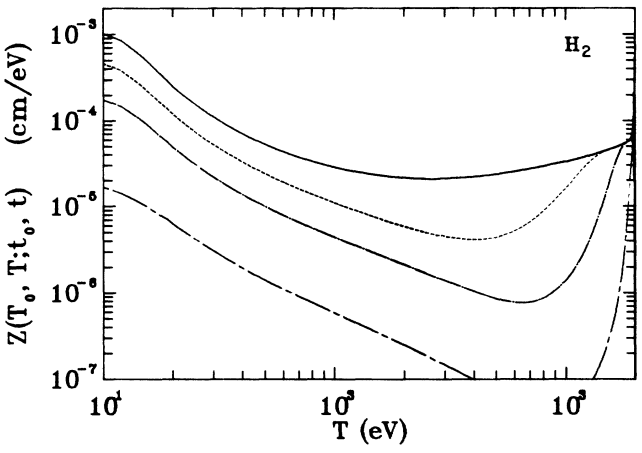

FIG. 1. Cumulative electron degradation spectrum $Z(T_0,T;t_0,t)$ in H_2 at the energy $T_0=2000$ eV of an incident electron entering at time $t_0=0$, plotted as a function of electron energy T. The chain-dashed curve represents the spectrum at 2 ns, the dash-dotted curve the spectrum at 8 ns, the dashed curve the spectrum at 16 ns, and the solid curve the spectrum at the stationary state, i.e., at $t\to\infty$.

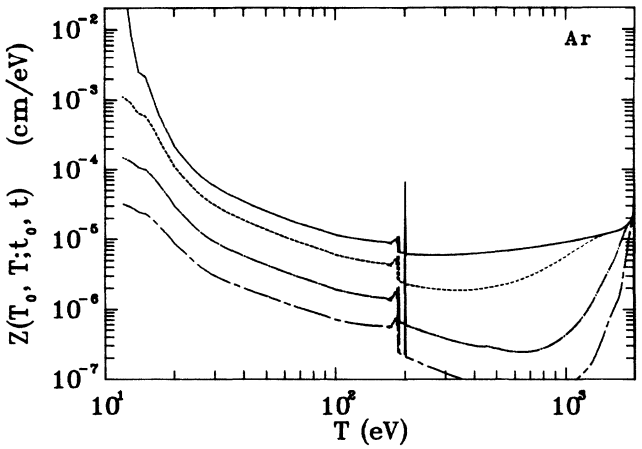

FIG. 2. Cumulative electron degradation spectrum $Z(T_0,T;t_0,t)$ in Ar resulting from an incident electron of energy $T_0=2000$ eV at time $t_0=0$, plotted as a function of electron energy T. The chain-dashed curve represents the spectrum at 1 ns, the dash-dotted curve the spectrum at 2 ns, the dashed curve the spectrum at 5 ns, and the solid curve the spectrum at the stationary state, i.e., at $t\rightarrow\infty$.

gy region.

While the stationary spectrum shows a rapid increase near the threshold energy of the lowest excitation, the cumulative degradation spectrum shows no such rapid increase until 5 ns. This result is understandable when we recall that the cumulative spectrum at $T\leq 20$ eV depends on the number of collisions at that energy. The number of collisions in Ar diminishes as T decreases to nearly the threshold energy, and therefore secondary electrons generated at these T values do not promptly contribute to the cumulative spectrum. A sharp peak at 200 eV due to Auger electrons following the L-shell ionization and complex structures below the peak (i.e., the Lewis effect due to the Auger electrons[27]) are clearly seen at the earliest time.

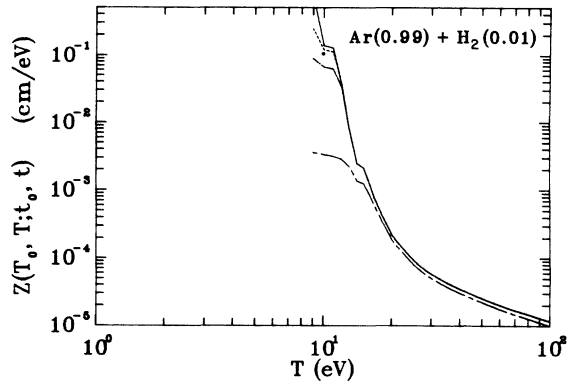

FIG. 3. Cumulative electron degradation spectrum $Z(T_0,T;t_0,t)$ in the Ar(0.99)+H_2(0.01) mixture below $T=100$ eV, for incident electron energy $T_0=2000$ eV. The chain-dashed curve represents the spectrum at 8 ns, the dash-dotted curve the spectrum at 100 ns, the dashed curve the spectrum at 300 ns, and the solid curve the spectrum at the stationary state, i.e., at $t\rightarrow\infty$.

Finally, we discuss the cumulative spectrum for the mixture. Because the mixture contains Ar at 99%, it is reasonable to expect that the cumulative spectrum is very close to that for pure Ar; in fact, it is nearly identical (Fig. 2) except for lower energies below 15 eV. Because the lowest electronic excitation energies are 8.8 eV for H_2 and 11.8 for Ar, special features of the cumulative spectrum for the mixture appear below 11.8 eV. To show details, we present in Fig. 3 an enlargement of the cumulative spectrum of $T\leq 100$ eV at later times. It is now more obvious that electrons with energies below 11.8 eV degrade much more slowly because the number of collisions is small. At 8 ns the cumulative spectrum does not rise rapidly below 15 eV. This is because the secondary electrons generated do not contribute to the cumulative spectrum immediately, as is understandable from Eq. (27). Even at 300 ns, the cumulative spectrum is slightly lower than the stationary spectrum below 11.8 eV. The stationary spectrum shows a mild slope below 11.8 eV, where the cross section for the $b\ ^3\Sigma_u^+$ excitation possesses a plateau (see Fig. 1 in Ref. 30).

2. *Cumulative yield spectrum for the Ar+H_2 mixture*

We plot $nTZ(T_0,T;t_0,t)\sigma_s(T)$ as a function of $\ln T$ and call this the cumulative yield spectrum for product s. The area under the curve in any energy interval represents contributions to the yield from that interval.

Figure 4 shows the cumulative yield spectrum for the M-shell ionization of Ar at different times. The spectrum shows a peak at 200 eV that is due to Auger electrons and complex structures below the peak. The cumulative yield spectrum at 1 ns has some contributions below 200 eV because secondary electrons generated in low energies join in further ionization at early times.

Figure 5 shows the cumulative yield spectrum for the $b\ ^3\Sigma_u^+$ state of H_2 at successive times. As is clear from the stationary yield spectrum, most of the yield of $b\ ^3\Sigma_u^+$ states occurs only below 20 eV, again pointing out an important role of subexcitation electrons in the mixture. At 2 ns the cumulative yield spectrum is very small, imply-

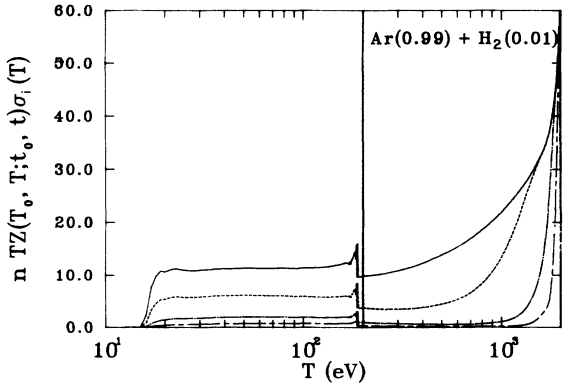

FIG. 4. Cumulative yield spectrum for the M-shell ionization of Ar in the Ar(0.99)+H_2(0.01) mixture. The chain-dashed curve represents the spectrum at 1 ns, the dash-dotted curve the spectrum at 2 ns, the dashed curve the spectrum at 5 ns, and the solid curve the spectrum at the stationary state, i.e., at $t\rightarrow\infty$.

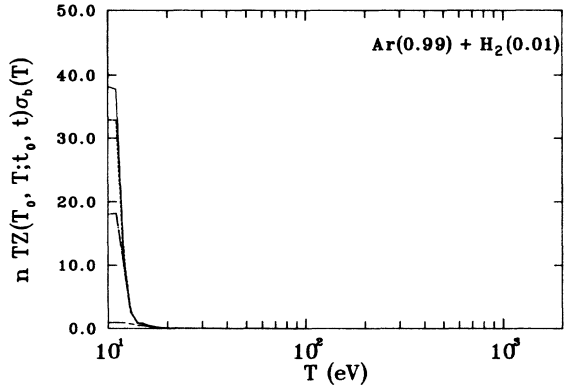

FIG. 5. Cumulative yield spectrum for the $b\,^3\Sigma_u^+$ excitation of H_2 in the $Ar(0.99)+H_2(0.01)$ mixture. The chain-dashed curve represents the spectrum at 8 ns, the dash-dotted curve the spectrum at 100 ns, the dashed curve the spectrum at 300 ns, and the solid curve the spectrum at the stationary state, i.e., at $t\rightarrow\infty$.

ing that subexcitation electrons have not started interacting appreciably with H_2 molecules. At 100 ns the peak of the cumulative yield spectrum becomes nearly half of the stationary spectrum, and by 300 ns the peak of the spectr a 87% of the stationary value.

3. *Time-dependent yield of ions, the $B\,^1\Sigma_u^+$ state, and the $b\,^3\Sigma_u^+$ state in pure H_2*

As shown in Fig. 6, the time-dependent yield of ions steadily increases until 27.5 ns and reaches the stationary value by 35 ns. The yield of the $B\,^1\Sigma_u^+$ state grows more rapidly than that of $b\,^3\Sigma_u^+$ at early times and reaches the stationary value at 35 ns, but that of the $b\,^3\Sigma_u^+$ state still shows a slight increase at that time. The faster growth of the yield of the $B\,^1\Sigma_u^+$ state is due to the larger cross section for excitation of this state at large T values.

4. *Time-dependent yields of ions and excitation in pure Ar*

Figure 7 shows the time-dependent yields of ions, the $1s_2+1s_4$ states, the $4p$ state, and the $1s_3+1s_5$ states of

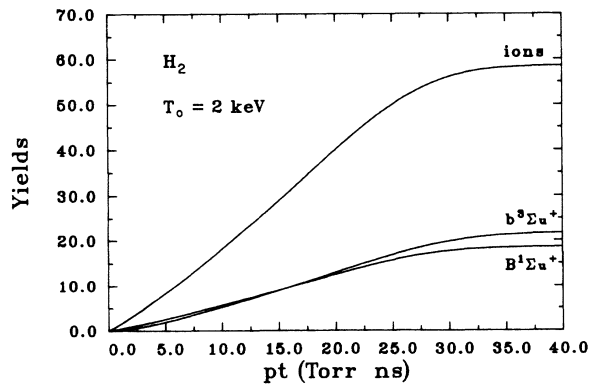

FIG. 6. Cumulative yields of ions, the $b\,^3\Sigma_u^+$ state, and the $B\,^1\Sigma_u^+$ state in pure H_2, plotted against time.

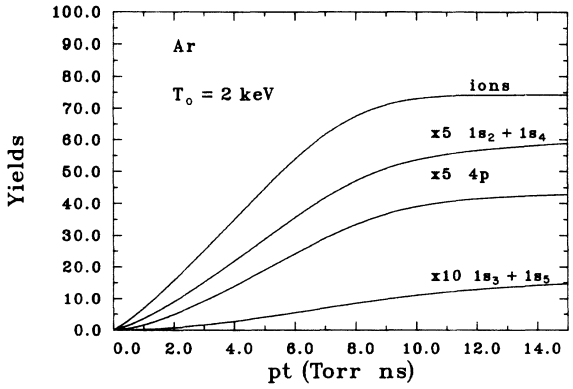

FIG. 7. Cumulative yields of ions, the $1s_2+1s_4$ states, the $4p$ state, and the $1s_3+1s_5$ states in pure Ar, plotted against time.

Ar. The yield of ions increases rapidly and almost reaches the stationary value at 11 ns. This period of 11 ns is about one-third of the corresponding period in H_2. The yield of the $1s_3+1s_5$ states is negligible until 1 ns and increases to reach saturation at 15 ns. The production of the $1s_2+1s_4$ states and the $4P$ states starts at $t=0$ and persists at 15 ns. It should be noted that the present results agree with our previous results[13] obtained by using a different procedure to solve the TDSF equation within a few percent.

5. *Time-dependent yields of ions and the $b\,^3\Sigma_u^+$ state of H_2 in the $Ar(0.99)+H_2(0.01)$ mixture*

Figure 8 shows the time-dependent yields of ions and the $b\,^3\Sigma_u^+$ state of H_2 in the mixture. The yield of ions rises rapidly and shows saturation at almost the same time as that in Ar, at 11 ns. By contrast, the yield of the $b\,^3\Sigma_u^+$ state increases gradually and does not show saturation even at 180 ns. The generation of the $b\,^3\Sigma_u^+$ state is almost entirely due to the subexcitation electrons and continues to take place at much later times. Indeed, the yield of the $b\,^3\Sigma_u^+$ state still increases at 500 ns (which is outside the range of Fig. 8) and is 9.62, which amounts to 89% of the stationary value.

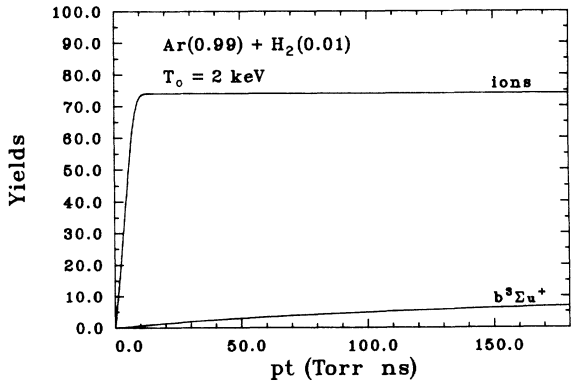

FIG. 8. Cumulative yields of ions and the $b\,^3\Sigma_u^+$ state of H_2 in the $Ar(0.99)+H_2(0.01)$ mixture, plotted against time.

6. *Energy distribution of electrons in the Ar(0.99)+H_2(0.01) mixture*

At the end of Sec. II D we pointed out that $(n v_T K_T + A)Z(T;t)$ represents the total number of electrons that have arrived at energy T by time t. For simplicity let us denote this quantity as $N(T;t)$. In what follows, Fig. 9 shows $N(T;t)$ specifically for the standard solution $Z(T_0,T;t_0,t)$, with $T_0=2$ keV and $t_0=0$, in the Ar(0.99)+H_2(0.01) mixture as a function of T at successive times. As time increases, $N(T;t)$ approaches a stationary value; indeed, by 8 ns, $N(T,t)$ at 8 ns and that of the stationary value are nearly identical. It is instructive to compare the cumulative spectrum with $N(T;t)$. As shown in Fig. 4, the cumulative spectrum at 8 ns is very close to its stationary value above 15 eV, but it is considerably lower below 15 eV. In other words, electrons below 15 eV do not contribute to the cumulative spectrum soon after they are generated. This is because the number of collisions is small below 15 eV and even smaller below 11.8 eV, where the electrons become subexcitation electrons.

C. Effect of momentum transfer to Ar on the degradation spectrum

An electron with energy between 11.8 and 8.8 eV loses its energy through the excitation of the $b\ ^3\Sigma_u^+$ state of H_2 and also through the momentum transfer upon elastic scattering with Ar. The role of the momentum transfer below 11.8 eV is evaluated in the following manner.

The mean energy E_m transferred per collision is $E_m=2mT/M$, where m is the mass of an electron and M the mass of Ar. Thus $E_m=2.75\times10^{-4}$ eV at $T=10$ eV, for example. The contribution to the stopping power from the momentum transfer of Ar is $0.99nE_m\sigma_m(T)=10.3$ eV/cm at 10 eV, where $\sigma_m(T)$ is the momentum-transfer cross section for Ar with a value[31] of 14.0×10^{-16} cm^2 at 10 eV. The corresponding contribution from the excitation of the $b\ ^3\Sigma_u^+$ state of H_2 is 238 eV/cm for an excitation cross section of 1.01×10^{-16} cm^2 at 10 eV. The ratio of the stopping-power contributions is 1/24. Therefore, we can safely conclude that the momentum transfer to Ar does not seriously influence the electron degradation between 11.8 and 8.8 eV in the mixture. However, the ratio is smaller in a mixture with lower H_2 concentration, and therefore it will be necessary to account for the momentum transfer to Ar explicitly.

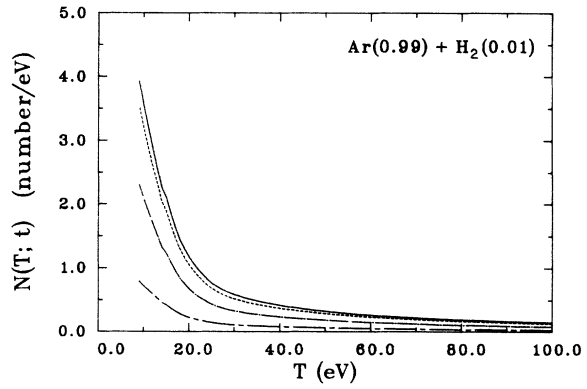

FIG. 9. Energy distribution of electrons that have reached energy T by time t in the Ar(0.99)+H_2(0.01) mixture. The chain-dashed curve represents the distribution at 2 ns, the dash-dotted curve the distribution at 5 ns, the dashed curve the distribution at 8 ns, and the solid curve the distribution at the stationary state, i.e., at $t\rightarrow\infty$.

D. Some remarks on secondary processes

All discussions above concern *initial processes* in which direct energy transfer takes place from primary and secondary electrons to individual atoms and molecules that constitute matter. The initial products thus formed start a series of reactions inducing exchange of energies and particles and hence chemical changes from the original matter. For instance, the ion-molecule reactions between Ar^+ and H_2, or Ar and H_2^+, are very fast, especially when the H_2^+ ion is in a vibrationally excited state. Therefore it is important to relate time scales of the initial and later processes. In the mixture of Ar and H_2, several reaction paths are available:

(I-1) $Ar^+ + H_2 \rightarrow ArH^+ + H$ chemical reaction

(I-2) $\rightarrow Ar + H_2^+$ charge transfer

(I-3) $Ar^+ + Ar \rightarrow Ar + Ar^+$ resonant charge transfer

or

(II-1) $Ar + H_2^+ \rightarrow ArH^+ + H$ chemical reaction

(II-2) $\rightarrow Ar^+ + H_2$ charge transfer .

Let us consider a homogeneous mixture of 99% Ar and 1% H_2 at 1 Torr and 0 °C so that the process (I) would have to be included in the present model. In a theoretical study[32] of reactions (I) and (II), the rate constant for reaction (I) was approximately determined as 6×10^{-11} cm^{3}s^{-1}/molecule at 0 °C. In addition, the resonant charge-transfer rate constant for (I-3) is known[33] approximately to be 2×10^{-10} cm^{3}s^{-1}/molecule. Using this information, along with the time-dependent yields of Ar^+ discussed in the preceding sections, we carried out chemical kinetic analysis to estimate the time scale of appearance of ArH^+ and H_2^+ species as secondary products by solving time-dependent, first-order coupled kinetic equations.[34] Although it may be tempting to suggest that as soon as Ar^+ ions are produced they interact with nearby Ar and H_2, sizable amounts of secondary products in (I) begin to appear in a time scale of 10^{-6} sec, which compares with 10^{-8} sec for the initial Ar^+ production. Thus secondary processes are important at a much later time than are primary processes.

The energy transfer from excited Ar to H_2 is known to play an important role for the production of $H_2(b\ ^3\Sigma_u^+)$ and this contribution should be explicitly evaluated. The processes considered are

(III-1) $Ar^* + H_2 \xrightarrow{k_{III}} Ar + H_2(a\ ^3\Sigma_g^+)$,

(III-2) $H_2(a\ ^3\Sigma_g^+) \xrightarrow{\tau_{III}} H_2(b\ ^3\Sigma_u^+) + h\nu$,

where k_{III} and τ_{III} are the rate constant and the radiative lifetime for (III-1) and (III-2), respectively, and are measured to have the respective values $8.2 \pm 0.4 \times 10^{-11}$ $cm^3\ s^{-1}$/molecule (Ref. 35) and 11 ns.[36] A simple calculation reveals that the production of $H_2(b\ ^3\Sigma_u^+)$ through processes (III-1) and (III-2) becomes appreciable only later at 10^{-6} sec in the (99% Ar+1% H_2) mixture. Therefore, this contribution to the $H_2(b\ ^3\Sigma_u^+)$ yield is negligible and that by subexcitation electrons is the sole cause of the $H_2(b\ ^3\Sigma_u^+)$ production at earlier times.

ACKNOWLEDGMENTS

This work was supported in part by the U.S. Department of Energy, Assistant Secretary for Energy Research, Office of Health and Environmental Research, under Contract No. W-31-109-Eng-38. We thank Y. Hatano for valuable discussion, including a remark that lead to the concluding paragraph.

*Present address: Department of Chemistry, University of British Columbia, Vancouver, British Columbia, Canada V6T 1Y6.

[1]W. P. Jesse and J. Sadauskis, Phys. Rev. **88**, 417 (1952).
[2]W. P. Jesse and J. Sadauskis, Phys. Rev. **90**, 1120 (1953).
[3]W. P. Jesse and J. Sadauskis, Phys. Rev. **97**, 1668 (1955).
[4]W. P. Jesse and J. Sadauskis, Phys. Rev. **100**, 1755 (1955).
[5]M. Inokuti, Radiat. Res. **59**, 343 (1974).
[6]R. L. Platzman, Radiat. Res. **2**, 1 (1955).
[7]T. E. Bortner and G. S. Hurst, Phys. Rev. **93**, 1236 (1954).
[8]G. S. Hurst and T. D. Strickler, *Penetration of Charged Particles in Matter,* Publication No. 753 (National Academy of Sciences, National Research Council, Washington, D.C., 1960), p. 134.
[9]T. D. Strickler, J. Phys. Chem. **67**, 825 (1963).
[10]E. Eggarter, J. Chem. Phys. **84**, 6123 (1986).
[11]M. Inokuti and E. Eggarter, J. Chem. Phys. **86**, 3870 (1987).
[12]M. Kimura and M. Inokuti, J. Chem. Phys. **87**, 3875 (1987).
[13]M. Inokuti, M. A. Dillon, and M. Kimura, Int. J. Quantum Chem. Symp. **21**, 251 (1987).
[14]M. A. Dillon, M. Inokuti, and M. Kimura, Radiat. Phys. Chem. **32**, 43 (1988).
[15]M. Inokuti, M. Kimura, and M. A. Dillon, Phys. Rev. A **38**, 1217 (1988).
[16]M. Inokuti, M. Kimura, and M. A. Dillon, Radiat. Phys. Chem. **34**, 477 (1989).
[17]R. Cooper, L. Denison, and M. C. Sauer, Jr., J. Phys. Chem. **86**, 5093 (1982).
[18]L. S. Denison, R. Cooper, and M. C. Sauer, Jr., J. Phys. Chem. **90**, 683 (1986).
[19]R. Cooper and M. C. Sauer, Jr., Radiat. Phys. Chem. **34**, 75 (1989).
[20]R. Cooper and M. C. Sauer, Jr., J. Phys. Chem. **93**, 1881 (1989).
[21]J. M .Warman, M. Zhou-lei, and D. van Lith, J. Chem. Phys. **81**, 3908 (1984).
[22]J. M. Warman, U. Sowada, and M. P. DeHaas, Phys. Rev. A **31**, 1974 (1985).
[23]K. Kowari, M. Kimura, and M. Inokuti, J. Chem. Phys. **89**, 7229 (1988).
[24]A. Pagnamenta, M. Kimura, M. Inokuti, and K. Kowari, J. Chem. Phys. **89**, 6220 (1988).
[25]M. A. Ishii, M. Kimura, M. Inokuti, and K. Kowari, J. Chem. Phys. **90**, 3081 (1989).
[26]M. A. Ishii, M. Kimura, and M. Inokuti (unpublished).
[27]K. Kowari, M. Kimura, and M. Inokuti, Phys. Rev. A **39**, 5545 (1989).
[28]D. A. Douthat, J. Phys. B **12**, 663 (1979).
[29]E. Eggarter, J. Chem. Phys. **62**, 833 (1975).
[30]M. Kimura, M. Inokuti, and K. Kowari, Phys. Rev. **40**, 2316 (1989).
[31]Y. Itikawa, At. Data Nucl. Data Tables **14**, 1 (1974).
[32]S. Chapman, J. Chem. Phys. **82**, 4033 (1985).
[33]R. E. Johnson, J. Phys. B **3**, 539 (1970).
[34]J. O. Hirschfelder, F. Curtiss, and R. B. Bird, *Molecular Theory of Gases and Liquids* (Wiley, New York, 1964), p. 441.
[35]A. Yokoyama, T. Ueno, and Y. Hatano, Chem. Phys. **22**, 459 (1977).
[36]R. E. Imhof and F. H. Read, J. Phys. B **4**, 1063 (1971).